Photonuclear reactions at intermediate energies investigated via the Monte Carlo multicollisional intranuclear cascade model

T. E. Rodrigues,[1] J. D. T. Arruda-Neto,[1,3] A. Deppman,[1] V. P. Likhachev,[1,*] J. Mesa,[1] C. Garcia,[1] K. Shtejer,[1] G. Silva,[1]
S. B. Duarte,[2] and O. A. P. Tavares[2]

[1]*Instituto de Física da Universidade de São Paulo, P.O. Box 66318, CEP 05315-970, São Paulo, Brazil*
[2]*Centro Brasileiro de Pesquisas Físicas-CBPF/MCT, 22290-180 Rio de Janeiro, Brazil*
[3]*Universidade de Santo Amaro / UNISA, São Paulo, Brazil*
(Received 6 February 2004; published 18 June 2004)

The Monte Carlo multicollisional (MCMC) intranuclear cascade model is used to study photonuclear reactions at intermediate energies ($20 \leqslant E_\gamma \leqslant 140$ MeV). This version of the code differs from previous versions in the following aspects: (i) the quasideuteron model of photoabsorption is consistently included by taking into account relative momentum correlations of the neutron-proton pair in a relativistic kinematics; (ii) a realistic treatment of the Pauli-blocking mechanism at the initial photoabsorption and at each binary nucleon-nucleon scattering during the cascade process is incorporated throughout the calculations; (iii) a criterion based on energy considerations is required by the end of the cascade. Differently from other transport models used so far, which are based on a randomly generated nuclear ground state with a stochastic treatment of the Pauli blocking, the present model incorporates a shell constrained momentum space of the nucleons which is preserved as the cascade evolves along time. The transition between the pre-equilibrium and evaporation phases is energetically determined, allowing the description of the cascade process without any free parameter, such as some ambiguous stopping time parameters adopted in similar time-structured cascade models. The occupation number distribution after the cascade corresponds to a typical Fermi distribution at a finite nuclear temperature, and the long-standing spurious depletion of the Fermi sphere, usually present in other cascade models, no longer appears. The Pauli-blocking factors are calculated and compared with previous approaches based on Fermi gas level density calculations. The evaporation-fission process of the compound nucleus is described in the framework of a Monte Carlo algorithm. Experimental data of the total photoabsorption cross section and the neutron multiplicities for Sn, Ce, Ta, and Pb in the 20–140-MeV range are described fairly well by the present calculations.

I. INTRODUCTION

In the last 40 years or so, intranuclear cascade models have been widely used to describe high-energy nucleon and photon-induced nuclear reactions. The long-standing conceptual difficulty is, however, the inclusion of in-medium quantum effects, such as the Pauli-blocking mechanism, into a semiclassical, many-body collisional process. The nuclear ground state is always generated from a uniform Fermi distribution of the momenta, with the spin and isospin degrees of freedom being artificially taken into account by the inclusion of statistical blocking factors, which presumably reproduce the nuclear quantum effects on the average. High-energy nucleon-induced reactions were widely studied by the intranuclear cascade model of Bertini [1], and also by the ISABEL code [2,3]. Bertini's INC model is based on a time independent approach, while in the ISABEL collisions between particles that were not promoted above the Fermi level are suppressed. These models have some disadvantages as the fate of all nucleons is not followed during the cascade, discarding, thus, the possibility of extracting information of physical observables at a given time.

Another important, and time-dependent intranuclear cascade model, the Liège-INC model, was first proposed to de-

scribe heavy-ion collisions in the GeV range [4], where a new version was introduced to deal with nucleon-nucleus reactions [5]. As reported in a recent work [6], this version needed some improvements, and another version was proposed [7]. This later one was reasonably successful in reproducing a large body of experimental data, by introducing what the authors called a self-consistent determination of the *stopping time* of the cascade process. On the other hand, systematic discrepancies were also observed, which were basically ascribed to the sharp nuclear surface approximation. Furthermore, this version incorporated the Pauli principle by means of statistical blocking factors, which led to some spurious depletion of the Fermi sea, as reported elsewhere [6], originating a small percentage of negative excitation energy cascade events. These unphysical events were considered as zero excitation energy events in the version INCL2 [7,8]. In the INCL3 code [9–11], the cascade process was forced to terminate just before the first collision leading to negative excitation energies. In a recent work [12], a *strict* Pauli blocking was incorporated, where collisions leading to nucleons with momentum smaller than the Fermi momentum were forbidden. It is clear that such blocking mechanism does not take into account the depletion of the Fermi sphere, and the experimental data suggest a blocking mechanism somewhere between these two different approaches [12]. A new version of the Liège-INC cascade model (INCL4) [6] was

*Deceased.

then proposed in order to describe the cascade process more realistically. In this version a diffuse nuclear surface is used, and it is also assumed that the excitation energy due to the rearrangement of the level occupations inside the Fermi sphere was not allowed to become negative. Such an assumption neglects the Fermi motion of particles with momentum lower than the Fermi momentum and, consequently, does not represent what is expected in actual nuclei. Furthermore, the version INCL4 contains an approach based on the classification of the nucleons into participants and spectators, where participants were particles that had collided with at least another participant, with the first participant being the incident particle that had started the cascade process. The spectator nucleons were the remaining particles, and were not allowed to collide between them. These restrictions were imposed in order to prevent against the so-called "spontaneous boiling" of the Fermi sphere, according to which nucleons close to the Fermi surface were able to gain energy through collisions between other spectators, and thus escape from the nucleus, even when the nucleus was not disturbed from its ground state. It is quite clear that this "spontaneous boiling" is a direct violation of the Pauli-exclusion principle.

Cascade calculations in photonuclear reactions have also been carried out using many different approaches: (i) isolated-particle interactions [1,13–15]; (ii) superposition of several independent one-body interactions [16–19]; and (iii) many-body cascade simulations [19,20]. In the isolated-particle mechanism the interactions between rescattered particles are not taken into account, while in the superposition approach the rapid and pre-equilibrium stage are not properly treated, since the ejection of fast nucleons is neglected. These two approaches are designated here as *conventional* cascade calculations. In the Monte Carlo multicollisional intranuclear cascade model (MCMC) [19,20], the semiclassical time evolution of all particles is followed in a many-body dynamics and the pre-equilibrium stage is naturally incorporated.

The present version of the shell-constrained MCMC model differs from the previous versions [19,20] in the following aspects: (i) the neutron-proton pairs are sorted, taking into account relative momentum correlations (quasideuteron model of photoabsorption [23–25]), and also including energy and momentum conservation in a relativistic kinematics; (ii) it incorporates a realistic treatment of the Pauli-blocking mechanism at the initial photoabsorption and at each binary nucleon-nucleon interaction without any free parameter; and (iii) a thermal equilibrium condition is imposed in order to stop the cascade. We show that this new and consistent approach circumvents all the shortcomings and drawbacks present in state of the art approaches so far developed [6–12]. We have focused our analysis on the description of photonuclear processes at intermediate photon energies $(20 \leqslant E_\gamma \leqslant 140$ MeV), since short-range correlations are expected to play a major role at these energies [26]. Furthermore, we also investigate the reliability of the intranuclear cascade model at the quasideuteron energy range.

The main goal of this new version of the MCMC model is the implementation, for the first time, of a realistic description of the cascade process with neither free parameters nor *ad hoc* assumptions, by only imposing physical constraints related to the Pauli-blocking mechanism. Even though it preserves the time structure of the code, a criterion based on energy conservation was also included to stop the cascade process. This procedure seems to be more reliable than simply choosing a *stopping time* to the cascade, which is usually adopted in similar calculations [6–12]. This *stopping time* is independent of the incident energy and also of the actual cascade history [6], representing an average time parameter to stop the cascade. In a more realistic picture, however, each cascade event has its own history, dictated by the initial interaction mechanism and by the dynamical evolution of the system.

This paper is divided into four sections. In Sec. II we describe the reformulated MCMC model, focusing on the initial photoabsorption mechanism, new implementation of the Pauli blocking, and thermal equilibrium criterion to stop the cascade. In this section we compare some physical values obtained in our calculations with other model predictions. The Pauli-blocking function in the QD model is also addressed. In Sec. III we compare our results with the available experimental data of the total photoabsorption cross section and the photoneutron multiplicities for Sn, Ce, Ta, and Pb in the 20–140-MeV range. A brief description of the evaporation process is also included. Finally, our conclusions are presented in Sec. IV.

II. THE SHELL-CONSTRAINED MONTE CARLO MULTICOLLISIONAL (MCMC) INTRANUCLEAR CASCADE MODEL

A. The multicollisional approach

The Monte Carlo multicollisional (MCMC) intranuclear cascade model is employed to describe the rapid stage of nuclear reactions, particularly photon-induced nuclear reactions at intermediate energies (20–140 MeV), the main focus of the present study. Nucleon-induced nuclear reactions, however, may also be accessed by just switching to the appropriate initial interaction mechanism.

In the many-body approach, all the particles are treated as participants and all the relevant processes are taken into account. At intermediate energies, however, only elastic nucleon-nucleon scattering takes place. As the initial photon is absorbed by an *n-p* pair inside the nucleus (QD model), the proton and the neutron are supposed to split and initiate two *correlated* cascade branches. The kinematics involved in the photoabsorption mechanism and the Pauli-blocking effects are discussed later. These two cascade branches are called *correlated* because all particles are allowed to collide between them, which is the premise of the MCMC model. As the system evolves in time, the fate of all particles is followed and the relativistic dynamics of the cascade is dictated by the splitting of the *n-p* pair and the actual history of the cascade event. Reflection and emission of particles at the nuclear surface are also taken into account. The energy balance during the emission of particles through the potential well is described in the Appendix.

The previous versions of the MCMC model have been widely used to describe photonuclear [19,20] and heavy-ions [21,22] reactions in the 0.5–1.5-GeV range. In these ver-

sions, the stochastic generation of the initial target configuration and the statistical approach to deal with Pauli-blocking effects led to some spurious negative excitation energy events, as reported in similar works [6–12]. The purpose of our new model is to eliminate these unphysical events and describe more realistically the time evolution of the fermionic system.

B. The initial target configuration

In the Fermi gas model the Fermi energy for protons, E_F^π, and neutrons, E_F^ν, is written as[1]

$$E_F^\pi = \frac{1}{2m_0}(3\pi^2)^{2/3}\hbar^2\left(\frac{Z}{\Omega}\right)^{2/3}, \quad \text{and} \tag{1}$$

$$E_F^\nu = \frac{1}{2m_0}(3\pi^2)^{2/3}\hbar^2\left(\frac{A-Z}{\Omega}\right)^{2/3}, \tag{2}$$

where $\Omega = \frac{4}{3}\pi r_0^3 A$ is the spherical, sharp surface, nuclear volume, and m_0 is the nucleon rest mass.

By using the relativistic, energy-momentum relationship $E^2 = p^2 + m_0^2$, where E and p are, respectively, the total energy and momentum of the nucleon (taking $\hbar = c = 1$), we write the corresponding on-shell Fermi momentum (k_F) as

$$k_F^\pi = \sqrt{E_F^\pi(E_F^\pi + 2m_0)}, \tag{3}$$

$$k_F^\nu = \sqrt{E_F^\nu(E_F^\nu + 2m_0)}. \tag{4}$$

The momenta of the nucleons are uniformly distributed inside a sphere of radius k_F^ν, which is the same as taking the bottom of the neutron well as the lowest energy level. The momenta of the neutrons are then sorted from zero to k_F^ν, and for protons from k_{min}^π to k_F^ν, where $k_{min}^\pi = k_F^\nu - k_F^\pi$.

In a completely analogous manner, the positions of the nucleons are uniformly distributed inside the nuclear volume, with $r_0 = 1.18$ fm.

The nucleons are bounded in a square-well potential defined as

$$V_0 = E_F^\nu + \text{binding}(\sim 7 \text{ MeV}), \tag{5}$$

where the binding energy and the nuclear radius parameter are the only two parameters of our calculations.

The binding effect of the potential V_0 is accounted for by means of the effective mass theory [27], according to

$$\sqrt{p^2 + m_0^2} - V_0 \equiv \sqrt{p^2 + m^{*2}}, \tag{6}$$

with m^* having the role of a nucleon effective mass. Equation (6) may be rewritten in the form

$$m^*(p) = \sqrt{m_0^2 + V_0^2 - 2V_0\sqrt{p^2 + m_0^2}}, \tag{7}$$

showing that m^* is dependent on the nucleon momenta. The value of m^* could be approximated to the corresponding average value $\langle m^* \rangle$

$$\langle m^* \rangle = \int_0^{k_F^\nu} m^*(p)F(p)dp, \tag{8}$$

where $F(p)dp = 3[p^2/(k_F^\nu)^3]dp$ is the probability of finding a nucleon with momentum between p and $p+dp$. For a Pb target, for example, this distribution yields $\langle m^* \rangle = 0.950m_0$. This value is in reasonable agreement with the parametrization of Ref. [28], where the value $m^* = (0.953 \pm 0.002)m_0$ is reported.

C. The photoabsorption mechanism

The dominant mechanism for nuclear photoabsorption at intermediate energies (40–140 MeV) is described by the so-called quasideuteron model [23–25]. This model has been employed to access the total photoabsorption cross section in heavy nuclei [29–31], and it is based on the assumption that the incident photon is absorbed by a correlated neutron-proton pair inside the nucleus, leaving the remaining nucleons as spectators. Such an assumption is enforced when one compares the relatively small wavelength of the incident photon with the nuclear dimensions. The nuclear photoabsorption cross section $\sigma_{QD}(E_\gamma)$ is then proportional to the available number of n-p pairs inside the nucleus (NZ), and also to the free-deuteron photodisintegration cross section $\sigma_d(E_\gamma)$

$$\sigma_{QD}(E_\gamma) = \frac{L}{A}NZ\sigma_d(E_\gamma)f(E_\gamma). \tag{9}$$

Here, the factor L/A represents the fraction of correlated n-p pairs [32,33], and the function $f(E_\gamma)$ accounts for the reduction of the n-p phase space due to the Pauli-exclusion principle. The Pauli-blocking function $f(E_\gamma)$ was theoretically calculated by Chadwick *et al.* [26] using Fermi-gas single-particle and two-particle state densities, and also imposing energy and momentum conservation to the proton and neutron final states. This analytic derivation for $f(E_\gamma)$ was an important improvement compared with previous phenomenological approaches [34,35], and should be verified in our calculations for a given target nucleus and photon energy. The free-deuteron photodisintegration cross section (expressed in mb) could be written as [36]

$$\sigma_d(E_\gamma) = \frac{61.2(E_\gamma - B)^{3/2}}{E_\gamma^3}, \tag{10}$$

where $B = 2.224$ MeV is the binding energy of the deuteron.

Levinger showed that the nuclear photoabsorption cross section is dependent on the quasideuteron wave function $\Psi_k(r)$ [23]. Accordingly

---

[1]The Fermi energy of protons and neutrons is different if the zero energy level is fixed at the bottom of the proton and neutron wells, respectively.

$$\Psi_k(r) = \left(\frac{4\pi}{\Omega}\right)^{1/2}\left[\frac{\sin(kr+\delta)}{\sin\delta} - \chi\right]r^{-1}(\alpha^2+k^2)^{-1/2}, \tag{11}$$

where r and k are, respectively, the relative position and momentum of the neutron-proton pair, δ is the phase shift, α^{-1} is the scattering length, and χ depends on the nuclear potential and plays a relevant role only inside the range of nuclear forces. This model also requires that the proton and neutron should be close enough to ensure that the wave function of the remaining $(A-2)$ nucleons is undisturbed after the initial interaction with the photon. From the theory of effective range [37,38], one can relate the phase shift δ with the scattering length α^{-1} by

$$\cot\delta \approx -\frac{\alpha}{k}. \tag{12}$$

For high-energy incident photons, which means the investigation of $\Psi_k(r)$ for small r and $kr\ll 1$, Eq. (11) takes the form

$$\Psi_k(r) \approx \left(\frac{4\pi}{\Omega}\right)^{1/2}(1-\alpha r-\chi)r^{-1}(\alpha^2+k^2)^{-1/2}, \tag{13}$$

where we have used Eq. (12). So, in the relevant region of small r, the wave function (13) is proportional to the deuteron ground-state wave function $\Psi_d(r)$, i.e.,

$$\Psi_d(r) = \left(\frac{2\alpha}{1-\alpha r_{\text{eff}}}\right)^{1/2}(e^{-\alpha r}-\chi)r^{-1}$$
$$\approx \left(\frac{2\alpha}{1-\alpha r_{\text{eff}}}\right)^{1/2}(1-\alpha r-\chi)r^{-1}, \tag{14}$$

since the common factors $(1-\alpha r-\chi)r^{-1}$ cancel out. The effective range r_{eff} was taken as 1.761 fm.

The quasideuteron photoabsorption cross section $\sigma_{qd}(k,E_\gamma)$ [note the difference between the photoabsorption cross section of a quasideuteron pair with relative momentum k, denoted by $\sigma_{qd}(k,E_\gamma)$ and the nuclear photoabsorption cross section in the QD model, denoted by $\sigma_{\text{QD}}(E_\gamma)$] can then be written in terms of the deuteron photodisintegration cross section $\sigma_d(E_\gamma)$ as

$$\frac{\sigma_{qd}(k,E_\gamma)}{\sigma_d(E_\gamma)} = \frac{|\Psi_k(r)|^2}{|\Psi_d(r)|^2} = \frac{2\pi(1-\alpha r_{\text{eff}})}{\Omega\alpha}\frac{1}{\alpha^2+k^2}. \tag{15}$$

The relation (15) was first obtained by Levinger [23], and indicates that the probability of photoabsorption is proportional to $(\alpha^2+k^2)^{-1}$, as also reported by other authors [26]. For that reason, in order to consistently generate an ensemble of quasideuteron candidates, we first sort neutron-proton pairs uniformly inside the nuclear volume and then reject those pairs whose relative momentum is not in agreement with the normalized probability $M_{qd}(k)$

$$M_{qd}(k) = \frac{\alpha}{\tan^{-1}\left(\frac{k_F^\nu}{\alpha}\right)}\frac{1}{\alpha^2+k^2} = \frac{\alpha}{\tan^{-1}\left(\frac{k_F^\nu}{\alpha}\right)}m_{qd}(k). \tag{16}$$

This procedure is equivalent to sort neutron-proton pairs whose relative momentum satisfies the overall photoabsorption probability $\Phi_{\gamma,\text{abs}}(k,k_F^\nu)$, where

$$\Phi_{\gamma,\text{abs}}(k,k_F^\nu) = N(k_F^\nu)M(k)m_{qd}(k), \tag{17}$$

and

$$M(k) = 24\frac{k^2}{(k_F^\nu)^3}\left[1-\frac{3k}{2k_F^\nu}+\frac{1}{2}\left(\frac{k}{k_F^\nu}\right)^3\right] \tag{18}$$

is the distribution of relative momenta of two nucleons in a Fermi gas [27], with the normalization $N(k_F^\nu)$ being given by

$$N(k_F^\nu) = \left\{\frac{3}{(k_F^\nu)^6}\left[-2\alpha^2(k_F^\nu)^2+3(k_F^\nu)^4+6\alpha^2(k_F^\nu)^2\ln(\alpha^2\right.\right.$$
$$\left.+(k_F^\nu)^2)+2\alpha^4\ln(\alpha^2+(k_F^\nu)^2)-8\alpha(k_F^\nu)^3\tan^{-1}\left(\frac{k_F^\nu}{\alpha}\right)\right.$$
$$\left.\left.-4\alpha^2(\alpha^2+3(k_F^\nu)^2)\ln\alpha\right]\right\}^{-1}. \tag{19}$$

The relativistic kinematics of photoabsorption is written as

$$P^{\text{Lab}} = P_{qd}^{\text{Lab}} + P_\gamma^{\text{Lab}} = P_\pi'^{\text{Lab}} + P_v'^{\text{Lab}}, \tag{20}$$

where P_{qd}^{Lab} and P_γ^{Lab} are the energy-momentum 4-vectors of the quasideuteron *candidate* (qd) and photon (γ), respectively. $P^{\text{Lab}}=(E^{\text{Lab}},\mathbf{p}^{\text{Lab}})$ is the energy-momentum 4-vector of the system $(qd+\gamma)$, all in the laboratory frame. The primes correspond to the final states of the neutron and proton after photoabsorption. The z axis was chosen for the direction of the incident photon in the laboratory frame.

Moving to the center of mass (c.m.) frame by an appropriate Lorentz transformation $\mathbf{L}(\beta)$, we write

$$P^{\text{c.m.}} = \mathbf{L}(\beta)P^{\text{Lab}} = P_{qd}^{\text{c.m.}} + P_\gamma^{\text{c.m.}} = (E^{\text{c.m.}},\mathbf{0}) = P_\pi'^{\text{c.m.}} + P_v'^{\text{c.m.}}, \tag{21}$$

where $\beta=\mathbf{p}^{\text{Lab}}/E^{\text{Lab}}$, and $E^{\text{c.m.}}$ is the total energy of the system in the c.m. frame. From Eq. (21) we write[2]

$$P_\pi'^{\text{c.m.}} = \left(\frac{E^{\text{c.m.}}}{2},\mathbf{q}\right) \quad\text{and} \tag{22}$$

$$P_\pi'^{\text{c.m.}} = \left(\frac{E^{\text{c.m.}}}{2},-\mathbf{q}\right), \tag{23}$$

where $\mathbf{q}$ is the momentum of the emitted proton in the c.m. frame, with $q=\sqrt{(E^{\text{c.m.}}/2)^2-\langle m^*\rangle^2}$. The angular coordinates

---

[2]Since there is no difference, in our model, between the neutron and proton rest masses, the total energy of the system in the c.m. frame is equally distributed between the members of the pair.
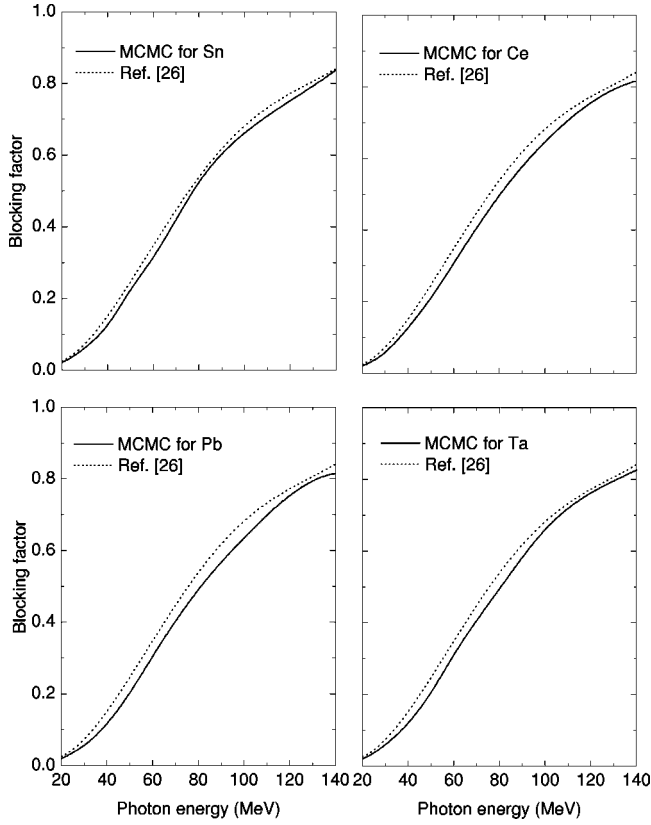
FIG. 1. Pauli-blocking functions $f(E_\gamma)$ for Sn, Ce, Ta, and Pb from MCMC (full lines) and Ref. [26] (dashed-lines).

FIG. 2. $\left|[f(E_\gamma)^{\mathrm{MCMC}}-f(E_\gamma)^{\mathrm{Ref.\,[24]}}]/f(E_\gamma)^{\mathrm{MCMC}}\right|$ for Sn, Ce, Ta, and Pb. Details in the text.

of the emitted proton (θ_π,φ_π) are then generated uniformly in a solid angle $d\Omega_\pi=\sin\theta_\pi d\theta_\pi d\varphi_\pi$.

The 4-vectors of the outgoing particles are those calculated back in the laboratory frame

$$P_\pi'^{\mathrm{Lab.}}=\mathbf{L}(-\beta)P_\pi'^{\mathrm{c.m.}}, \qquad (24)$$

$$P_\nu'^{\mathrm{Lab.}}=\mathbf{L}(-\beta)P_\nu'^{\mathrm{c.m.}}. \qquad (25)$$

After the photoabsorption, if both proton and neutron have momentum higher than the Fermi momentum, the quasideuteron *candidate* is finally *selected*, and the cascade process is initiated. On the contrary, this photoabsorption is Pauli-blocked, and we have to choose another quasideuteron *candidate* inside the nuclear volume. The competition between blocked and nonblocked events is directly related to the phase-space reduction due to the Pauli-blocking mechanism, and is a consistent way to determine the Pauli-blocking function for a given target and photon energy. This procedure is somewhat at variance with the one reported in a recent work [39], where the nucleons effective masses are left as free parameters and the sorting procedure does not take into account relative momentum correlations. In Fig. 1 we show our calculations (full lines) of $f(E_\gamma)$ for Sn, Ce, Ta, and Pb in the 20–140-MeV range, in comparison with the prediction of Chadwick and collaborators [26] (dotted lines). Figure 2 shows the absolute value of their relative difference: $\left|[f(E_\gamma)^{\mathrm{MCMC}}-f(E_\gamma)^{\mathrm{Ref.\,[24]}}]/f(E_\gamma)^{\mathrm{MCMC}}\right|$. As easily noticed,

our results indicate that the heavier the nucleus, the stronger the blocking factor, as one would expect from the exclusion principle. Furthermore, our calculations show stronger blocking factors in the entire energy range when compared with the results of Ref. [26]. Note that both calculations have an overall agreement better than 10% from 80 MeV on. The relative difference is higher for lower photon energies, where the Pauli principle is expected to play a major role. Such higher suppression should be interpreted as a consequence of a more rigorous blocking mechanism once the MCMC explicitly takes into account the actual particle levels, instead of using the level densities.

D. The realistic nonstochastic Pauli blocking

The neutron and proton, following the initial photoabsorption (QD model), trigger two *correlated* cascade branches, where the fate of all particles is dictated by the initial interaction mechanism and by the dynamics of the system.

The Pauli-exclusion principle is elegantly incorporated during the cascade by the inclusion of spherically symmetric nuclear shells in the momentum space of the nucleons. Such shell-constrained approach implies that the maximum number of protons or neutrons with momentum between p and $p+\Delta p$ should not exceed the actual number of nucleons occupying this shell at the initial target configuration. The depletion of the Fermi sphere is naturally taken into account at each binary nucleon-nucleon scattering by blocking those collisions every time one or both nucleons have closed-shell final states. In the event of a nonblocked collision, the occupation numbers are updated, otherwise the particles do not interact, and we look for the next event in the cascade process.

The momentum-interval Δp, inherent to our model, represents a gap in momentum space that accommodates a multiple of the actual (continuum) nucleon momentum, and should be interpreted as a momentum uncertainty. Such momentum interval is calculated by the uncertainty relationship $\Delta p\Delta r\sim\hbar/2$, where Δr was taken to be the nuclear radius,
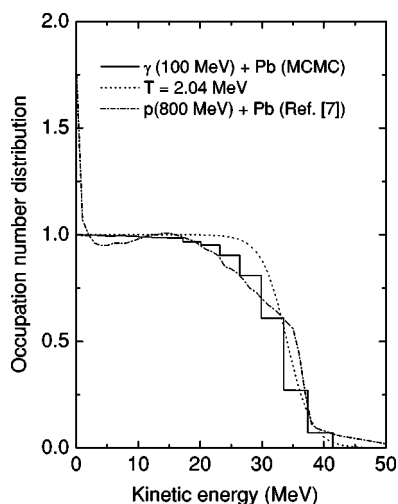
FIG. 3. Occupation number distribution of the remaining nucleons as a function of the kinetic energy after the cascade $\gamma(100\ \text{MeV})+\text{Pb}$ from the MCMC model (histogram), in comparison with the Liège-INC model (dashed line, adapted from Ref. [7]) for the cascade $p(800\ \text{MeV})+\text{Pb}$. The dotted line is a typical Fermi distribution of a complete degenerated Fermi gas at a fixed temperature ($T=2.04$ MeV), equivalent to the average excitation energy $\langle E^*\rangle$ from the MCMC output.

once there are no restrictions to the positions of the nucleons. For a heavy nucleus, such as ^{208}Pb, we found $\Delta p \sim 14$ MeV/c.

This physical constraint naturally eliminates all the spurious events related to the miss-treatment of the Pauli-blocking mechanism, such as the spontaneous boiling of the Fermi sphere reported by Boudard *et al.* [6]. Furthermore, our many-body collisional model propitiates a realistic description of the cascade process, since all particles are allowed to interact with each other, and thus the Fermi sphere is repopulated by any nucleon inside the nuclear volume. Similar transport models [6–12] used up to now allow this repopulation only by participants, which is the same as neglecting the Fermi motion of particles not active in the cascade.

The reliability of our Pauli-blocking mechanism is verified in Fig. 3, where we show the occupation number distribution (solid histogram) of the remaining nucleons after the cascade $\gamma(100\ \text{MeV})+\text{Pb}$, as a function of the nucleon's kinetic energy, in comparison with the Liège-INC [7] calculations (dashed line) for the cascade $p(800\ \text{MeV})+\text{Pb}$. The dotted line is the calculation for a typical Fermi distribution of a complete degenerated Fermi gas at a fixed temperature ($T=2.04$ MeV) equivalent to the average excitation energy $\langle E^*\rangle$ from the MCMC output. The chemical potential is compatible with the compound nucleus configuration. The agreement between the actual occupation number distribution and the theoretical prediction for a complete degenerated Fermi gas illustrates the accuracy of our calculations. In the Liège-INC model, however, we note a stronger depletion of particles just below the Fermi energy, and also a nonphysical, higher than unit, occupation number at low kinetic energy. Such cooling behavior indicates, probably, that the energy of the system is being miss-shared with the most energetic

nucleons, which are escaping from the nucleus, leading to inaccurate values of some important evaporation parameters, such as the compound nucleus excitation energy (E^*). We emphasize that, as also pointed out by Cugnon *et al.* [7], all the cascade models used up to now show the same discrepancies, which are physically eliminated in our model.

E. The energetic criterion to stop the cascade process

The time-dependent character of our model permits the continuous evaluation of physical observables as the cascade event evolves in time. Similar time-structured transport models [6–12] include a *stopping time* parameter to interrupt the cascade. Such *stopping time* is independent of the energy of the incoming particle and also represents an average value of time in which some quantities, like the excitation energy, change the way they very in time and the system is presumably at thermal equilibrium [6]. There is much ambiguity to determine this *stopping time*, since different physical observables give different time parameters. Furthermore, this average *stopping time* could be suitable for a specific cascade event, while for another it could be too short or too long to delineate the pre-equilibrium phase.

The rapid stage of a nuclear reaction is associated with a period of time when at least one particle has enough kinetic energy to escape from the nucleus. Such physical constraint implies that, when all the particles have kinetic energy lower than the potential depth, the system is at thermal equilibrium and the evaporation stage is about to initiate. This energetic criterion is employed in our model by checking the kinetic energy of all bounded nucleons every time that we have a nucleon-nucleon or a nucleon-surface interaction. In the event of all bounded nucleons having kinetic energy lower than the potential depth, the cascade process is terminated and the system is in thermal equilibrium (compound nucleus). This energetic criterion means that each cascade event has its own time of equilibrium, representing a significant improvement to describe the cascade process without *extra parameters*.

The excitation energy after the cascade process is calculated, following the prescription of older versions of the code [19,20] as

$$E^*(\text{MeV}) = E_\gamma - \sum_j (T_j^0 + B), \qquad (26)$$

where E_γ is the incident photon energy in the laboratory frame, T_j^0 is the asymptotic kinetic energy of the emitted nucleon j, and $B \sim 7$ MeV is the mean binding energy of the nucleons lying at the Fermi surface.

In Fig. 4 we show the normalized excitation energy distributions for the cascade $\gamma+^{209}\text{Bi}$ at 140 MeV from the MCMC model calculations (solid histograms) and from Ref. [40] (dashed histograms). The result obtained in Ref. [40] clearly exhibits a broader shape with an average photoexcitation energy $\langle E^*\rangle \sim 78$ MeV (dashed arrow) higher than the one achieved from the MCMC model $\langle E^*\rangle \sim 46$ MeV (solid arrow). The difference between these results could be ascribed to the Pauli-blocking mechanism, indicating that in our approach the depletion of the Fermi sphere is more re-
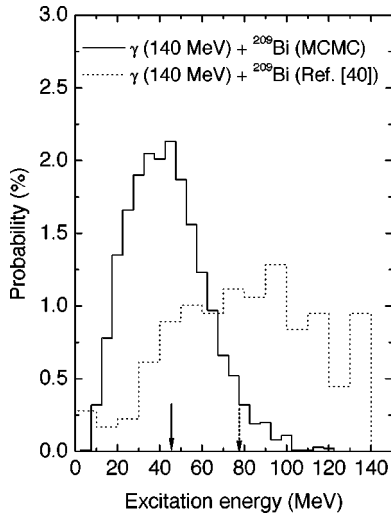
FIG. 4. Excitation energy distribution at the end of the cascade $\gamma(140 \text{ MeV}) + ^{209}\text{Bi}$ from the MCMC model (solid histogram) and Ref. [40] (dashed histogram). The solid and dashed arrows indicate the average excitation energies $\langle E^* \rangle$ from MCMC and Ref. [40], respectively.

strictive, leading to a narrower distribution with a lower and more accurate average value. Note also that the MCMC excitation energy distribution could be characterized by two distinct processes: (i) low final state interaction events at excitation energies up to approximately 50 MeV, where the distribution shows structures which are probably associated with the energy levels of the split neutron-proton pair; and (ii) high final state interaction events at higher excitation energies, corresponding to the Maxwellian-type descent inherent to highly randomized systems. Such randomization is associated with long time of equilibrium cascade events. The time of equilibrium and compound nucleus mass distributions for the cascade $\gamma+\text{Pb}$ at 100 MeV are shown in Fig. 5.

The difficulty found by similar time-dependent transport models [6–12] to achieve an energetic stopping criterion could be associated with the spurious depletion observed in
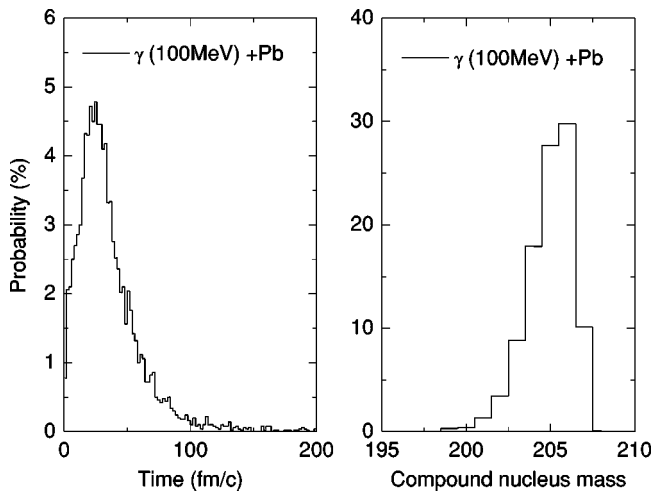

FIG. 5. Time of equilibrium and compound nucleus mass distributions for the cascade $\gamma(100 \text{ MeV})+\text{Pb}$ from MCMC calculations.

Fig. 3, since the system apparently never reaches a thermally equilibrated state. In that sense, we have combined some basic features of commonly used intranuclear cascade codes into an improved model, which physically incorporates a more appropriated Pauli-blocking mechanism with a consistent energetic criterion to stop the cascade, keeping, however, the time-dependent character of the routine.

III. COMPARISON WITH EXPERIMENT

The total photoabsorption cross section in the 20–140-MeV range is written as the sum of a quasideuteron (QD) and a giant dipole resonance (GDR) contribution

$$\sigma_T(E_\gamma) = \sigma_{\text{QD}}(E_\gamma) + \sigma_{\text{GDR}}(E_\gamma). \qquad (27)$$

The QD contribution is calculated from (9) with $L=6.5$ [26], and using the shapes of $f(E_\gamma)$ shown as full lines in Fig. 1. The GDR contribution is that of a Lorentz curve whose parameters were compiled elsewhere [41]. The results for $\sigma_T(E_\gamma)$ are shown in Fig. 6 (full lines), in comparison with the calculations of Ref. [26] (dotted lines). The data points were taken from Ref. [29]. The quantities designated by χ^2_{red} (χ^2 over the number of data points) are calculated for $E_\gamma \geqslant 25$ MeV to illustrate the statistical importance of both calculations. For Sn and Ta, both calculations have no statistical significance, while for Ce and Pb, the MCMC model better describes the data, including the more accentuated descent of the cross sections of Sn, Ce, and Pb up to approximately 50 MeV, suggesting a stronger blocking mechanism than the one calculated in Ref. [26].

The average neutron multiplicities $\langle \nu \rangle$ are also calculated, taking into account the two major contributions to the total photoabsorption cross section

$$\langle \nu \rangle = \frac{\sigma_{\text{QD}}(E_\gamma)}{\sigma_T(E_\gamma)} [\langle \nu \rangle_f + \langle \nu \rangle_s^{\mathcal{CN}}] + \frac{\sigma_{\text{GDR}}(E_\gamma)}{\sigma_T(E_\gamma)} \langle \nu \rangle_s^{\mathcal{T}}, \qquad (28)$$

where $\langle \nu \rangle_f$ and $\langle \nu \rangle_s$ are, respectively, the average fast and slow neutron multiplicities. The labels $\mathcal{CN} \equiv (A_{\mathcal{CN}}, Z_{\mathcal{CN}}, E^*_{\mathcal{CN}})$ and $\mathcal{T} \equiv (A_T, Z_T, E_\gamma)$ represent the compound nucleus and target configurations, respectively. $E^*_{\mathcal{CN}}$ is the average excitation energy of all cascade processes leading to the same compound nucleus $(A_{\mathcal{CN}}, Z_{\mathcal{CN}})$. The average excitation energy $\langle E^* \rangle$ as a function of E_γ is then given by

$$\langle E^* \rangle = \sum_{\mathcal{CN}} E^*_{\mathcal{CN}} \Gamma_{\mathcal{CN}}, \qquad (29)$$

where $\Gamma_{\mathcal{CN}}$ is the respective branching ratio for the $\mathcal{CN}$ formation.

The quantities $\langle \nu \rangle_f$, $E^*_{\mathcal{CN}}$, and $\Gamma_{\mathcal{CN}}$ are calculated in the framework of the MCMC model. Results for $\langle E^* \rangle$ and $\langle \nu \rangle_f$ for Sn, Ce, Ta, and Pb in the 20–140-MeV range are shown in Figs. 7 and 8, respectively.

The evaporation process is described by a Monte Carlo algorithm which calculates, at each step l of the evaporation chain, the competition between particle emission and nuclear
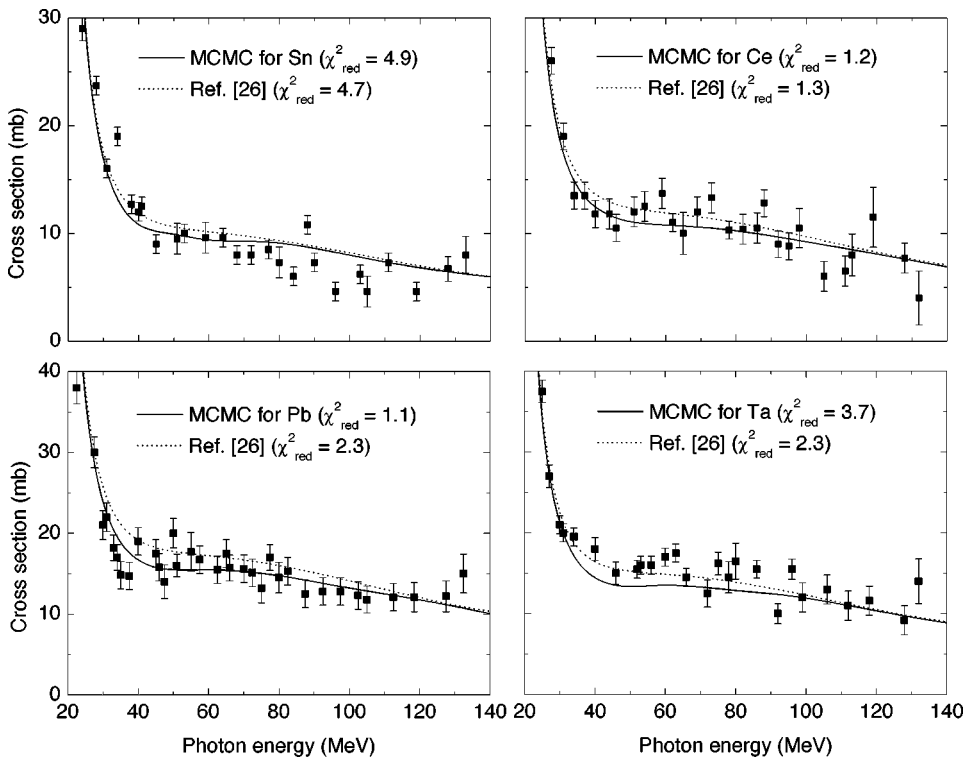
FIG. 6. The total photoabsorption cross section for Sn, Ce, Ta, and Pb from MCMC (full lines) and Ref. [26] (dashed lines). The data points are taken from Ref. [29]. See the text for details.

fission. This model is an improved version of the former *MCEF* code (for details see Refs. [42,43]) and is the subject of a forthcoming paper. Here, we briefly describe it for completeness.

The model takes into account the emission of neutron (n), proton (p), alpha (α), deuteron (d), tritium (t), and helium-3 (^{3}He). Shell-model corrections to the nuclear masses are also included [44].

The emission probability of particle k relative to neutron emission is calculated according to the Weisskopf's statistical model [45]

$$\frac{\Gamma_k}{\Gamma_n} = \left(\frac{\gamma_k}{\gamma_n}\right)\left(\frac{E_k^*}{E_n^*}\right)\left(\frac{a_k}{a_n}\right)\exp\{2[(a_k E_k^*)^{1/2} - (a_n E_n^*)^{1/2}]\},$$

(30)

where $(\gamma_k/\gamma_n) = 1(k=p)$, $2(k=\alpha)$, $1(k=d)$, $3(k=t)$, and $2(k=^3\text{He})$ [46]. $E_k^* = E^* - (B_k + V_k)$ is the nuclear excitation energy after the emission of particle k. The particles' binding energies B_k and the Coulomb potentials V_k are taken from Ref. [43].

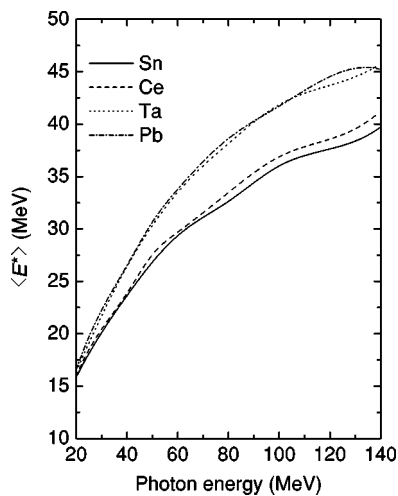The level density parameter for neutron emission is [47]

FIG. 7. Average photoexcitation energy for Sn, Ce, Ta, and Pb, as a function of the incident photon energy.
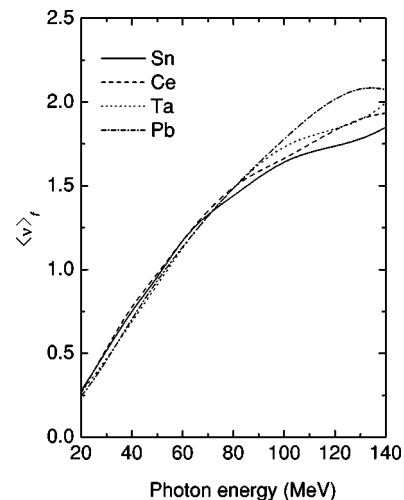

FIG. 8. Average number of fast neutrons emitted during the cascade stage for Sn, Ce, Ta, and Pb, as a function of the incident photon energy.
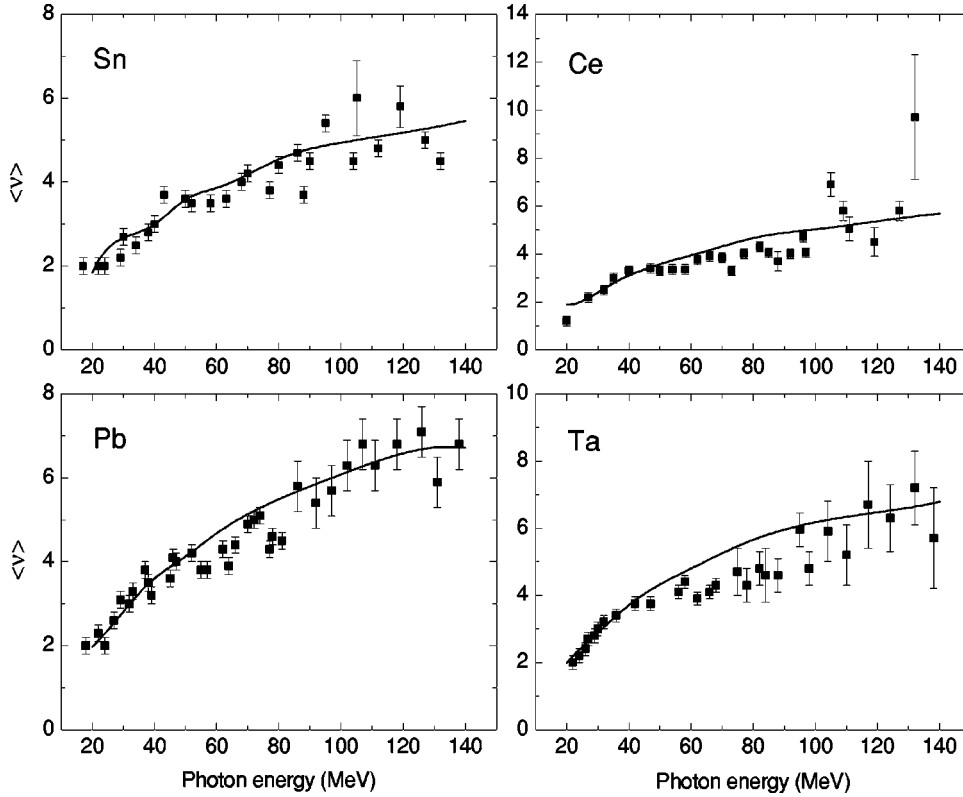
FIG. 9. Average neutron multiplicities for Sn, Ce, Ta, and Pb from MCMC+evaporation (full lines). The data points were taken from Ref. [30].

$$a_n = (0.134A - 1.21 \times 10^{-4}A^2)$$
$$\times \left\{ 1 + [1 - \exp(-0.061E^*)]\frac{\Delta M}{E^*} \right\}, \qquad (31)$$

where $\Delta M(\text{MeV})$ is the shell-model correction [44]. We have also adopted $a_k = a_n$ for the other particles' emissions [46].

The probability of fission relative to neutron emission is calculated using the LDM by Bohr and Wheeler [48] and the statistical model of Weisskopf [45] and Vandenbosch and Huizenga [49]

$$\frac{\Gamma_f}{\Gamma_n} = \frac{15a_n[2(a_f E_f^*)^{1/2} - 1]}{4A^{2/3}a_f E_n^*} \exp\{2[(a_f E_f^*)^{1/2} - (a_n E_n^*)^{1/2}]\},$$
$$(32)$$

with $E_f^* = E^* - B_f$.

The fission barrier B_f was taken from Ref. [43], while for a_f we have used [47]

$$a_f = \left[1 + 0.059\,17\left(\frac{Z^2}{A} - 34.34\right) \right]a_n, \quad \frac{Z^2}{A} \geq 34.9,$$
$$(33)$$

$$a_f = \left[1 + 0.0833\left(\frac{Z^2}{A} - 30.30\right) \right]a_n, \quad 31.20 < \frac{Z^2}{A} \geq 34.9,$$
$$(34)$$

$$a_f = a_n, \quad \frac{Z^2}{A} \leq 31.20. \qquad (35)$$

During the evaporation, the quantities A, Z, and ΔM are updated and the relative widths are recalculated. The process stops whenever fission occurs or when the available excitation energy is too low to evaporate a particle.

The slow neutrons multiplicities are then calculated by

$$\langle \nu \rangle_s^{\mathcal{CN}} = \sum_{\mathcal{CN}} \left[\frac{1}{N}\sum_{i=1}^{N} n_i^{\mathcal{CN}} \right]\Gamma_{\mathcal{CN}} \quad \text{and} \qquad (36)$$

$$\langle \nu \rangle_s^{T} = \frac{1}{N}\sum_{i=1}^{N} n_i^{T}, \qquad (37)$$

where the quantities $n_i^{\mathcal{CN}(T)}$ represent the total number of emitted neutrons for a given compound nucleus (target) configuration after the i-evaporation process is terminated and N is the number of evaporation histories. Direct neutron emissions from the GDR decay are unlikely to occur in heavy nuclei and were neglected in the calculation; thus, we have assumed $E^* = E_\gamma$.

The results are shown in Fig. 9, in comparison with the experimental data of Ref. [30]. The quite good agreement between theory and experiment is evident, including the two distinct regimes that show up from 20 to approximately 80 MeV and from 80 MeV on. This fact indicates that some important evaporation parameters, such as, $\langle \nu \rangle_f$, $E_{\mathcal{CN}}^*$, and $\Gamma_{\mathcal{CN}}$, were accurately determined. It should be stressed that the Pauli-blocking mechanism plays a very important role, as it dictates how the incoming energy flux is shared among the particles during the cascade. A strict Pauli blocking (blocking mechanism that suppresses collisions if the interacting particles do not have final momentum higher than the Fermi

momentum), like the one used in Bertini's code [1], has the effect of decreasing the excitation energy, since most collisions are forbidden and the depletion of the Fermi sphere is not taken into account. On the other hand, a stochastic Pauli blocking, like the one used in Liége-INC [6–12] and also in Ref. [40], tends to overestimate the excitation energy (see Fig. 4), because spurious depletion of the Fermi sphere are taking place, with the incident flux being kept almost entirely inside the nucleus. This result seems to be in contradiction with similar cascade calculations for hadron-induced reactions, where the stochastic Pauli blocking tends to decrease the average excitation energy slightly in comparison with the strict Pauli blocking (see Ref. [8]). So, in order to give a possible interpretation on that, we discuss below the effect of two different methods to interrupt the cascade: (i) using stopping-time parameters, or (ii) using an energetic condition.

Using stopping-time parameters with a stochastic Pauli blocking may introduce systematic errors in some physical observables, including the excitation energy, as the cascade evolves along time. For instance, the extending of the cascade process beyond the "correct" time of equilibrium will decrease the excitation energy, due to the spurious emissions caused by the unphysical repopulation of the Fermi sphere. Such spurious events were already reported and named spontaneous boiling for the case where the target nucleus is not excited but still can emit particles [6]. We point out that such cooling mechanism may be related to the discrepancies in the occupation number distribution shown in Fig. 3. A strict Pauli-blocking mechanism, however, will not allow such spurious emissions and will lead to higher excitation energies as reported in Ref. [8]. On the other hand, if the cascade is stopped prematurely, the excitation energy will be in excess for both approaches (stochastic/strict).

The use of an energetic method like the one discussed in this paper, plus a stochastic Pauli-blocking criterion, tends to increase the excitation energy when compared with the strict one, because the energy distribution mechanism is more "efficient" due to a much higher FSI of the triggered particles with the others during the cascade. The fate of this system is to approach a thermally equilibrated and highly excited state. A strict Pauli blocking will decrease the excitation energy simply because the active particles carry away a major portion of the incident energy.

IV. CONCLUSION

In this work we have proposed an extended version of the MCMC model to describe photonuclear reactions at intermediate energies. The quasideuteron model of photoabsorption includes relative momentum correlations during the sorting procedure, taking into account that the photon will most probably interact with *n-p* pairs with small relative momentum k, as suggested by Levinger's model [23]. The relativistic photoabsorption kinematics was accomplished by imposing energy and momentum conservation to the photon + quasideuteron system. The Pauli-blocking function was consistently determined for a given target and photon energy and shows an overall agreement, better than 10%, with the theo-

retical prediction by Chadwick *et al.* [26] for $E_\gamma \gtrsim 80$ MeV. For lower photon energies, however, our calculations show a much stronger blocking factor (see Figs. 1 and 2), which is partially supported by the experimental data of photoabsorption cross section. This difference is probably attributed to the fact that using level densities, instead of treating the Fermi gas levels explicitly, softens the Pauli-blocking effects. Note also that in our approach the nuclear finite size is naturally taken into account, and the blocking mechanism now depends on the target atomic and mass number.

The dynamical Pauli-blocking mechanism at multiple nucleon-nucleon scattering during the cascade evolution is rigorously incorporated by allowing collisions only if both final states are not already occupied, as imposed by the exclusion principle. This self-consistent physical approach circumvents the long-standing difficulty of dealing with in-medium effects in intranuclear cascade calculations, and eliminates all unphysical events related to the spurious depletion of the Fermi sphere (see Refs. [6–12]). The occupation number distribution (Fig. 3) corresponds approximately to a typical Fermi distribution at the end of the cascade, evidencing our better treatment of the dynamical Pauli-blocking effects *vis-à-vis* other transport models, which show remarkable discrepancies at low kinetic energies [7].

The refined treatment of the emission process (see the Appendix) and the inclusion of an energetic criterion to stop the cascade, propitiated the description of the cascade stage without any free parameter, such as stopping-time parameters commonly used in similar time-dependent cascade calculations [6–12].

In summary, the present MCMC has proven to be quite consistent with the experimental data of the total photoabsorption cross section and the neutron multiplicities for Sn, Ce, Ta, and Pb, in the 20–140-MeV range, serving as a stringent test for the cascade model at a wide energy and mass range, as far as the initial interaction mechanism is suitably described by a two-body interaction.

ACKNOWLEDGMENTS

APPENDIX: ENERGY BALANCE DURING PARTICLE EMISSION

In this section we show how to accurately perform the energy balance during the emission of a baryon j through the potential border. Tunneling of the Coulomb barrier is also taken into account for the case of charged particle emission. The calculations are carried out assuming that particles outside the potential border do not interact between them and with bounded particles, and also that the recoil of the nucleus is negligible. These assumptions substantially simplify our analysis, yet do not introduce a significant amount of error to the calculations. The first assumption is encouraged provided the distinction between bounded and unbounded particles is solely attributed to the nucleon rest mass [27]. For that rea-

son, every time that a baryon reaches the nuclear boundary with kinetic energy higher than the potential depth, it simply escapes from the nucleus with its corresponding free-nucleon mass, leaving it slightly cooler due to the mass deficit. The second assumption introduces an error of about $1/A_{\rm rem}$ ($A_{\rm rem}$ is the mass number of the bounded system) in the momentum p_j of the outgoing nucleon. For $A_{\rm rem} \gtrsim 100$ such error can be neglected. Furthermore, the recoil of the remaining nucleus as a whole does not change the relative velocity of the particles and, consequently, does not alter the cascade dynamics.

The energy and momentum conservation during the emission of nucleon j implies

$$\sum_{i \in A_{\rm rem}} \mathbf{P}_i = \sum_{i \in A_{\rm rem}(i \neq j)} \mathbf{P}'_i + \mathbf{P}'_j, \qquad (A1)$$

where the sums go over all bounded nucleons, with the $\mathbf{P}_i$'s representing the 4-vectors of the i nucleon. The primes correspond to the same quantities after the emission process.

The 3-vector components of Eq. (A1) are automatically satisfied within the above approximations. The remaining scalar component is then written in the form

$$\sum_{i \in A_{\rm rem}(i \neq j)} (p_i^2 + \langle m^* \rangle^2)^{1/2} + (p_j^2 + \langle m^* \rangle^2)^{1/2}$$
$$= \sum_{i \in A_{\rm rem}(i \neq j)} (p_i^2 + \langle m'^* \rangle^2)^{1/2} + (p_j^2 + m_0^2)^{1/2}. \quad (A2)$$

The sums in Eq. (A2) can be replaced by an average energy value $\langle E \rangle$ multiplied by $A_{\rm rem}$. So, rewriting Eq. (A2), one gets

$$A_{\rm rem} \langle E \rangle = A_{\rm rem} \langle E' \rangle + \xi, \qquad (A3)$$

where

$$\langle E \rangle = \int_0^{k_F^\nu} (p^2 + \langle m^* \rangle^2)^{1/2} F(p) dp, \qquad (A4)$$

$$\langle E' \rangle = \int_0^{k_F^\nu} (p^2 + \langle m'^* \rangle^2)^{1/2} F(p) dp, \qquad (A5)$$

and

$$\xi = (p_j^2 + m_0^2)^{1/2} - (p_j^2 + \langle m^* \rangle^2)^{1/2}, \qquad (A6)$$

where k_F^ν is the Fermi momentum equivalent to the $A_{\rm rem}$ nucleons.

All the quantities in Eq. (A3) are known, except $\langle m'^* \rangle$. So, assuming that $\langle m'^* \rangle$ is proportional to $\langle m^* \rangle$, i.e., $\langle m'^* \rangle = (1 - \delta)\langle m^* \rangle$, Eq. (A3) takes the form

$$\int_0^{k_F^\nu} [p^2 + (1 - \delta)^2 \langle m^* \rangle^2]^{1/2} F(p) dp$$
$$= \int_0^{k_F^\nu} (p^2 + \langle m^* \rangle^2)^{1/2} F(p) dp - \frac{\xi}{A_{\rm rem}}. \qquad (A7)$$

Since $\xi / A_{\rm rem} \ll \langle E \rangle$, we have $\delta \ll 1$. So, expanding the first square root and collecting terms in first order of δ

$$[p^2 + (1 - \delta)^2 \langle m^* \rangle^2]^{1/2} \approx (p^2 + \langle m^* \rangle^2 - 2\delta \langle m^* \rangle^2)^{1/2}$$
$$\approx \left(1 - \frac{\delta \langle m^* \rangle^2}{p^2 + \langle m^* \rangle^2} \right) (p^2 + \langle m^* \rangle^2)^{1/2}. \qquad (A8)$$

Inserting (A8) into (A7)

$$\int_0^{k_F^\nu} \left(1 - \frac{\delta \langle m^* \rangle^2}{p^2 + \langle m^* \rangle^2} \right) (p^2 + \langle m^* \rangle^2)^{1/2} F(p) dp$$
$$- \int_0^{k_F^\nu} (p^2 + \langle m^* \rangle^2)^{1/2} F(p) dp = - \frac{\xi}{A_{\rm rem}} \qquad (A9)$$

$$\therefore \delta \langle m^* \rangle^2 \int_0^{k_F^\nu} (p^2 + \langle m^* \rangle^2)^{-1/2} F(p) dp = \frac{\xi}{A_{\rm rem}}. \quad (A10)$$

Integrating Eq. (A10) and solving for δ, one finally obtains

$$\delta = \frac{\xi(k_F^\nu)^3}{3\langle m^* \rangle^2 A_{\rm rem}} \left\{ \frac{k_F^\nu}{2}((k_F^\nu)^2 + \langle m^* \rangle^2)^{1/2} - \frac{\langle m^* \rangle^2}{2} \ln[k_F^\nu + ((k_F^\nu)^2 + \langle m^* \rangle^2)^{1/2}] + \frac{\langle m^* \rangle^2}{2} \ln(\langle m^* \rangle) \right\}^{-1}. \qquad (A11)$$

The procedure outlined above is then applied every time a baryon is ejected from the nucleus, with the masses of the remaining nucleons being updated by the relation $\langle m'^* \rangle = (1 - \delta)\langle m^* \rangle$. The accuracy of this energy balance is of hundreds of keVs, representing less than 0.0010% of the total energy of a system with $A_{\rm rem} \gtrsim 100$.

---

[1] H. W. Bertini, Phys. Rev. Lett. **131**, 1801 (1963).
[2] Y. Yariv and Z. Fraenkel, Phys. Rev. C **20**, 2227 (1979).
[3] Y. Yariv and Z. Fraenkel, Phys. Rev. C **24**, 488 (1981).
[4] J. Cugnon, T. Mizutani, and J. Vandermeulen, Nucl. Phys. **A352**, 505 (1981).
[5] J. Cugnon, Nucl. Phys. **A462**, 751 (1987).
[6] A. Boudard, J. Cugnon, S. Leray, and C. Volant, Phys. Rev. C **66**, 044615 (2002).
[7] J. Cugnon, C. Volant, and S. Vuillier, Nucl. Phys. **A620**, 475 (1997).
[8] S. Leray et al., Phys. Rev. C **65**, 044621 (2002).
[9] J. Benlliure et al., Nucl. Phys. **A700**, 469 (2002).
[10] W. Wlazlo et al., Phys. Rev. Lett. **84**, 5736 (2000).
[11] C. Toccoli, Ph.D. thesis, University of Orsay, 2000.

[12] J. Cugnon and P. Henrotte, Eur. Phys. J. A **16**, 393 (2003).

[13] V. S. Barashenkov, F. G. Gereghi, A. S. Iljinov, G. G. Jonsson, and V. D. Toneev, Nucl. Phys. **A231**, 462 (1974).

[14] T. A. Gabriel, Phys. Rev. C **13**, 240 (1976).

[15] T. Sato, K. Shin, S. Ban, Y. Namito, H. Nakamura, and H. Hirayama, Nucl. Instrum. Methods Phys. Res. A **437**, 471 (1999).

[16] Th. Lamparter *et al.*, Z. Phys. A **355**, 1 (1996).

[17] R. C. Carrasco, M. J. Vicente Vacas, and E. Oset, Nucl. Phys. **A570**, 701 (1994); R. C. Carrasco, E. Oset, and L. L. Salcedo, *ibid.* **A541**, 585 (1992).

[18] L. L. Salcedo, E. Oset, M. J. Vicente-Vacas, and C. Garcia-Recio, Nucl. Phys. **A484**, 557 (1988).

[19] M. G. Gonçalves, S. de Pina, D. A. Lima, W. Milomen, E. L. Medeiros, and S. B. Duarte, Phys. Lett. B **406**, 1 (1997).

[20] S. de Pina, E. C. de Oliveira, E. L. Medeiros, S. B. Duarte, and M. G. Gonçalves, Phys. Lett. B **434**, 1 (1998).

[21] E. L. Medeiros, S. B. Duarte, and T. Kodama, Phys. Lett. B **203**, 205 (1988).

[22] M. G. Gonçalves, E. L. Medeiros, and S. B. Duarte, Phys. Rev. C **55**, 2625 (1997).

[23] J. S. Levinger, Phys. Rev. **84**, 43 (1951).

[24] J. S. Levinger, *Nuclear Photo-Disintegration* (Oxford University Press, Oxford, 1960), p. 97.

[25] J. S. Levinger, Phys. Lett. **82B**, 181 (1979).

[26] M. B. Chadwick, P. Oblozinský, P. E. Hodgson, and G. Reffo, Phys. Rev. C **44**, 814 (1991).

[27] K. Kikuchi and M. Kawai, *Nuclear Matter and Nuclear Reactions* (North-Holland, Amsterdam, 1968).

[28] C. A. Garcia Canal, E. M. Santangelo, and H. Vucetich, Phys. Rev. Lett. **53**, 1430 (1984).

[29] A. Leprêtre, H. Beil, R. Bergère, P. Carlos, J. Fagot, A. De Miniac, and A. Veyssière, Nucl. Phys. **A367**, 237 (1981).

[30] A. Leprêtre, H. Beil, R. Bergère, P. Carlos, J. Fagot, A. Veyssière, and I. Halpern, Nucl. Phys. **A390**, 221 (1982).

[31] A. Leprêtre *et al.*, Nucl. Phys. **A472**, 533 (1987).

[32] F. Murgia and P. Quarati, Mod. Phys. Lett. A **4**, 1 (1989).

[33] P. C. Stein, A. C. Odian, A. Wattenberg, and R. Weinstein, Phys. Rev. **119**, 348 (1960).

[34] M. Prakash, P. Braun-Munzinger, J. Stachel, and N. Alamanos, Phys. Rev. C **37**, 1959 (1988).

[35] W. M. Alberico, M. Ericson, and A. Molinari, Ann. Phys. (N.Y.) **154**, 356 (1984).

[36] J. R. Wu and C. C. Chang, Phys. Rev. C **16**, 1812 (1977).

[37] H. A. Bethe, Phys. Rev. **76**, 38 (1949).

[38] H. A. Bethe and C. Longmire, Phys. Rev. **77**, 647 (1950).

[39] S. de Pina, J. Mesa, A. Deppman, J. D. T. Arruda-Neto, S. B. Duarte, E. C. de Oliveira, O. A. P. Tavares, E. L. Medeiros, M. Goncalves, and E. de Paiva, J. Phys. G **28**, 2259 (2002).

[40] C. Guaraldo, V. Lucherini, E. De Sanctis, A. S. Iljinov, M. V. Mebel, and S. Lo Nigro, Nuovo Cimento Soc. Ital. Fis., A **103A**, 607 (1990).

[41] S. S. Dietrich and B. L. Berman, At. Data Nucl. Data Tables **38**, 199 (1988).

[42] A. Deppman, O. A. P. Tavares, S. B. Duarte, E. C. de Oliveira, J. D. T. Arruda-Neto, S. R. de Pina, V. P. Likhachev, O. Rodriguez, J. Mesa, and M. Gonçalves, Phys. Rev. Lett. **87**, 182701 (2001).

[43] A. Deppman, O. A. P. Tavares, S. B. Duarte, E. C. de Oliveira, J. D. T. Arruda-Neto, S. R. de Pina, V. P. Likhachev, O. Rodriguez, J. Mesa, and M. Gonçalves, Comput. Phys. Commun. **145**, 385 (2002).

[44] W. D. Myers and W. T. Swiatecki, Ark. Fys. **36**, 343 (1967).

[45] V. F. Weisskopf, Phys. Rev. **52**, 295 (1937).

[46] K. J. LeCouteur, Proc. Phys. Soc., London, Sect. A **63**, 259 (1950).

[47] O. A. P. Tavares and M. L. Terranova, Z. Phys. A **343**, 407 (1992).

[48] N. Bohr and J. A. Wheeler, Phys. Rev. **56**, 426 (1939).

[49] R. Vandenbosch and J. R. Huizenga, *Nuclear Fission*, 1st ed. (Academic, New York, 1973).